



TECHNICAL ARTICLE

Effect of Ti Addition on the Microstructure and Corrosion Resistance of AlCrCuFeNiNb_{0.2} High-Entropy Alloy

XUEWEI LIANG,¹ YUNHAI SU,^{1,2} TAISEN YANG,¹ ZHIYONG DAI,¹
and YINGDI WANG¹

1.—School of Materials Science and Engineering, Shenyang University of Technology, Shenyang 110870, China. 2.—e-mail: su_yunhai@sut.edu.cn

With rapid developments in industry, the unique design of high-entropy alloys (HEAs) has become a research hotspot in the field of corrosion. In this work, AlCrCuFeNiNb_{0.2}Ti_x HEAs were prepared through flux-cored wire and deposited on the surface of low-carbon steel by gas metal arc welding (GMAW). The effect of Ti on the phase structure and corrosion resistance of AlCrCuFeNiNb_{0.2}Ti_x HEA surfacing layer is discussed in detail. The results demonstrate that the microstructure of the surfacing layer was mainly composed of BCC solid solution with Fe-Cr phase and FCC solid solution with tiny amounts of MC phase. The microstructure presents the typical dendritic (DR) and interdendritic (ID) structures. It indicates that the addition of Ti can significantly promote the corrosion resistance of the surfacing layer. The corrosion resistance effect is stronger than that of 304 stainless steel. With the continuous addition of Ti, the self-corrosion current density of polarization curve decreases, the capacitance impedance radius of electrochemical impedance spectroscopy (EIS) increases, and the corrosion resistance of the surfacing layer improves. In the low-frequency region of EIS, there is an inductance component with pitting tendency. When the addition was Ti_{0.8}, the corresponding corrosion resistance value of the surfacing layer impedance was the smallest.

INTRODUCTION

Ocean engineering has great potential for economic and social development; however, the economic losses caused by the corrosion of mechanical equipment continue to increase. Therefore, it is very important to improve the corrosion resistance of metals. The appearance of high-entropy alloys (HEAs) meets, to a certain extent, the requirements of mechanical equipment surface material properties.¹

HEAs have a high degree of disorder, multi-components and simple phase structure. Through reasonable composition design,^{2–6} alloy materials with higher hardness, higher wear resistance, higher corrosion resistance, higher temperature oxidation resistance, and excellent mechanical and

electromagnetic properties can be obtained.^{7–12} Therefore, HEAs have general application prospects in corrosion- and wear-resistant tools, biomaterials, superalloys, electro-magnetic materials, and other fields. Zhang et al.¹³ prepared AlCoCrFeNiTi_x HEAs with single BCC structures for the first time. The alloys show excellent room-temperature compressive mechanical properties. However, there is a lack of research on corrosion performance. Tang et al.¹⁴ compared the corrosion rates of three kinds of HEAs with other alloys in 3.5% NaCl solution. The results indicated that the corrosion rate of CoCrFeNi HEA was equivalent to that of stainless steel and Al alloy, less than the rates of some Ni alloys, and significantly lower than that of low-carbon steel and low-alloy steel. Lin et al.¹⁵ studied the corrosion resistance of Cu_{0.5}CoCrFeNi HEAs as-cast and as-aged at different temperatures in 3.5% NaCl solution, and compared it with 304L stainless steel. The results showed that the passivation zone can be observed in the as-cast and as-aged alloys at

different temperatures. Due to the segregation of Cu, a galvanic cell is formed. The HEA easily forms a dense protective film, which can effectively enhance its corrosion resistance.

The Ti atomic radius is relatively large, and adding it to the HEA can increase the lattice distortion effect. And its configuration entropy value is higher, which can improve the hardness and strength of the alloy. It is conducive to the formation of BCC structure. Ti is an easy passivation metal. When the alloy is in the passivation state, a dense oxide film easily forms on the surface of the alloy, which has excellent corrosion resistance. Therefore, a high-entropy alloy with Ti has great potential for development. The mechanical properties and corrosion resistance of Ti-containing HEAs were studied in references.^{16–19} However, the bulk high-entropy alloy is mainly made by vacuum arc furnace smelting and melting casting.^{20,21} If a part of the casting fails, surfacing remanufacturing technology is used for repair. Most elements in high-entropy alloys are expensive, so re-surfacing can reduce the cost. Therefore, it is important for practical applications to be able to prepare a bulk HEA surfacing layer on low-cost carbon steel plate. Therefore, a new method of alloy preparation is adopted in this paper: preparing AlCrCuFeNiNb_{0.2}-Ti_x HEA surfacing layers by gas metal arc welding (GMAW). The phase structure and microstructure of the HEA surfacing layers are discussed, and the relationship between phase structure and corrosion resistance is discussed.

EXPERIMENTAL MATERIALS AND METHODS

Preparation of the Surfacing Layer

Firstly, according to the composition design of AlCrCuFeNiNb_{0.2}Ti_x ($x = 0.2, 0.6, 0.8$), we selected 120-mesh spherical powder with purity greater than 99.9%. Al, Cr, Cu, Ni, Nb, and Ti metal powders were used as the flux core, and Fe came completely from the steel strip of flux-cored wire. The powder needs to be dried in advance, because it easily absorbs moisture, and flux-cored wire produced with wet powder causes defects such as pores and cracks in the weld.¹⁸

Secondly, the alloy powder was weighed, and the filling rate was tested. The filling rate of the powder was 40%. At the start of the flux-cored wire control system, the powder falls into the U-shaped steel

strip, and after multi-pass rolling and drawing, the flux-cored wire has a diameter of 2.4 mm. At the same time, the reducing ratio can be controlled to 15–20%. The final proportions were Ti_{0.2}, Ti_{0.6}, and Ti_{0.8}. The composition of the steel strip and substrate are shown in Table I.

Finally, the substrate carbon steel surface was polished to remove oxide scale, cleaned with absolute ethanol, and then overlaid onto the carbon steel plate surface by GMAW to obtain AlCrCuFeNiNb_{0.2}-Ti_x HEAs. The welding process parameters²² are shown in Table II. Wire cutting produced a surfacing layer of 10 mm × 10 mm × 10 mm, and then microstructure observation and electrochemical detection was completed.

Experimental Methods

Before testing, the surfacing layer was polished and the phase composition of the surfacing alloy was investigated by x-ray diffraction. The specific parameters were: pure copper target, voltage 40 kV, current 30 mA, step size 4°/min, scanning range 20° to 90°. The phase composition of the surfacing layer was characterized by a Geminisem 300 field emission scanning electron microscope equipped with electron backscatter diffraction (EBSD) and an energy dispersive spectrometer (EDS). The electrode chemistry curve and AC impedance of the HEA overlay in 3.5% NaCl solution were measured by a VSP-300 electrochemical workstation, using a saturated calomel electrode as the reference electrode and a platinum electrode as the auxiliary electrode, with a scanning speed of 10 mV/min.

RESULTS AND DISCUSSION

Phase Structure

Figure 1 shows the XRD pattern of AlCrCuFeNiNb_{0.2}Ti_x HEA surfacing layers. As can be seen from Fig. 1a, the phase structures of Ti_{0.2}, Ti_{0.6}, and Ti_{0.8} HEA surfacing layers are relatively simple, and are composed of BCC phase and FCC phase. The three main peaks of the surfacing layer confirm that the substrate phase is BCC phase, accounting for the main proportion. By comparing the PDF cards, the substrate phase is consistent with Fe-Cr phase. It was proved that Fe-Cr phase solid solution is formed in the process of surfacing. Then, there are small diffraction peaks near $2\theta = 40.837^\circ$, $2\theta = 49.602^\circ$, and $2\theta = 72.108^\circ$ [a partial magnification is shown in Fig. 1b]. The diffraction intensity was lower and the content was less, and (Nb,Ti)C multiple-phase with FCC structure was found by PDF card comparison.²³ As shown in Fig. 1c, with the continuous addition of Ti element, the content of Ti in (Nb,Ti)C reaches saturation, excess Ti is incorporated into the BCC solid solution, and solute atoms with a large atomic radii cause lattice distortion. It can be seen from the Bragg equation that the (110) diffraction peak angle of the BCC

Table I. Compositions of H08A steel strip and substrate (wt.%)

	C	Si	Mn	S	P	Fe
H08A	0.03	0.01	0.30–0.55	0.013	0.011	Bal.
Substrate	0.20	0.35	0.70	0.045	0.045	Bal.

Table II. Welding process parameters

Welding current (A)	Arc voltage (V)	Welding speed (cm/min)	Gas flow (L/min)
160	24	8	12

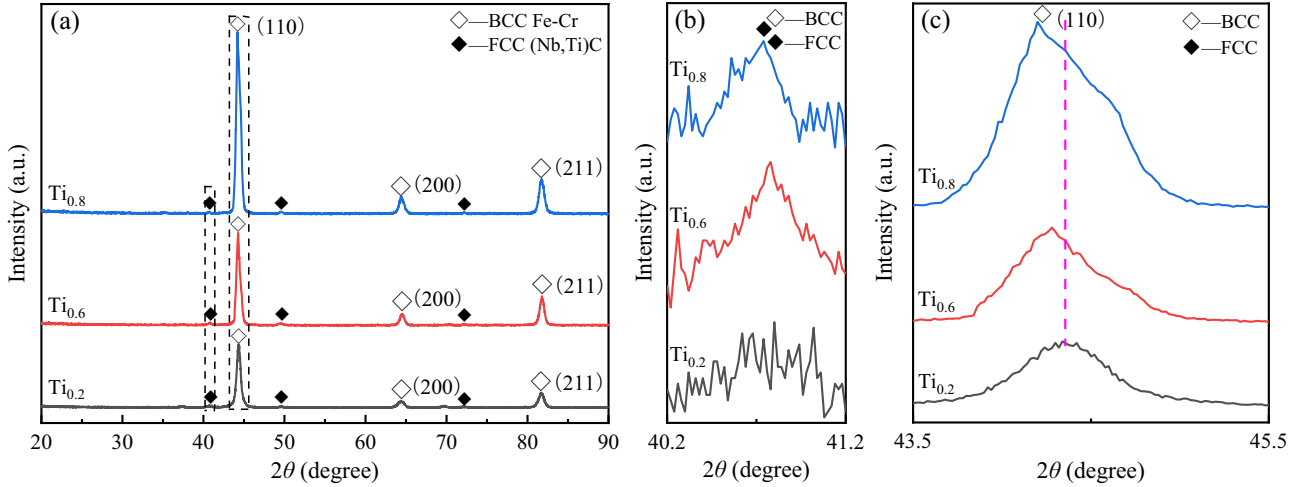


Fig. 1. X-ray diffraction of the AlCrCuFeNiNb_{0.2}Ti_x HEAs; (a) overall images, (b) locally enlarged images of FCC, (c) locally enlarged images of BCC.

phase in the HEA surfacing layer shifts slightly to the left with the continuous addition of Ti.^{24,25}

Figure 2 shows the EBSD phase diagram and phase histogram of AlCrCuFeNiNb_{0.2}Ti_x HEA surfacing layers. The phase structure of the surfacing layer consists of solid solution phase and uncertain phase; the solid solution phase includes BCC phase and a tiny amount of FCC phase. In Fig. 2a, c, and e, the red area represents BCC phase, occupying most of the region; the blue and chartreuse areas represent FCC phase. The overlapping of green and yellow indicates that FCC is a compound (Nb,Ti)C with small size and dispersed uniformly in the BCC substrate. In Fig. 2b, d, and f, with the continuous addition of Ti element, BCC phase is still dominant in the surfacing layer, while FCC phase increases slowly. When Ti content is 0.8, the proportion of BCC phase is 97.81%, FCC phase is 1.06%, and the ratio of BCC to FCC phase is 92.27. In conclusion, the addition of Ti is conducive to the formation of BCC phase, and can promote the simplification of phase structure, which is of great significance to the improvement of corrosion resistance.

Microstructures

Figure 3 shows the microstructure of AlCrCuFeNiNb_{0.2}Ti_x HEA surfacing layers. The typical gray dendrite (DR) and white interdendritic (ID) structures are clearly visible in the surfacing layer. In addition, there are some fine precipitates in the structure, which are evenly distributed. There are

no surface microcracks, slag inclusion, or pores in the structure of the surfacing layer. Table III shows the chemical composition of the different regions. The results show that in the microstructure of Ti_{0.2}, Ti_{0.6}, and Ti_{0.8} HEA surfacing layers, DRs are rich in Cr, Fe, Ni, and depleted Cu, while IDs are rich in Cu, Nb, and Ti. Due to the high heat input during the welding process, part of the Al element is burned and the transition coefficient is reduced. Under the action of high heat input, the substrate is diluted, and Fe element diffuses from the substrate to the surfacing layer, resulting in an increase in Fe element content.²³ Combined with XRD analysis, it can be seen that Nb and Ti have a strong ability to form carbides, and the massive precipitates in area A are (Nb,Ti)C. Moreover, fine (Nb,Ti)C particles are dispersed in the microstructure.²⁶ BCC solid solution becomes the matrix phase, and with the continuous addition of Ti element, the excess Ti is solid-dissolved into the matrix, and its content increases.

Corrosion Resistance

Figure 4 shows the electrochemical polarization curves of AlCrCuFeNiNb_{0.2}Ti_x HEA surfacing layers and 304 stainless steel in 3.5% NaCl solution. The corrosion system is composed of surfacing layer alloy and NaCl solution. Metal as the anode loses electrons and dissolves continuously. Compared with the 304 stainless steel, HEA surfacing layers have better corrosion resistance. With the

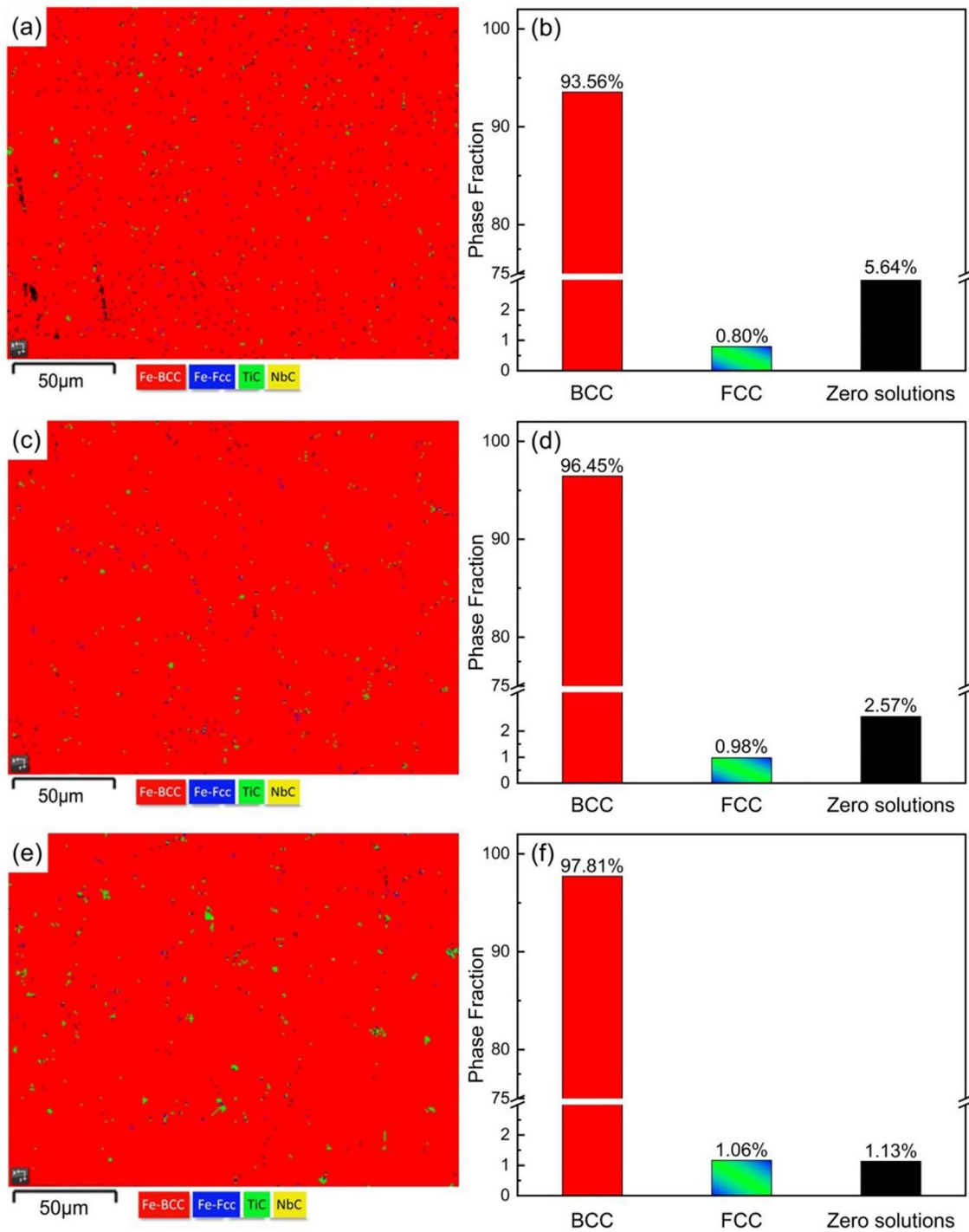


Fig. 2. EBSD phase maps and histograms of the phase of AlCrCuFeNiNb_{0.2}Ti_x HEAs; (a) and (b) Ti_{0.2}, (c) and (d) Ti_{0.6}, (e) and (f) Ti_{0.8} (Color figure online).

continuous addition of Ti element, the corrosion current decreases, and the corrosion rate of the alloy steady declines. As shown in Table IV, the corrosion resistance of Ti_{0.8} is the most significant. The self-corrosion current density continuously decreases to $9.9586 \times 10^{-5} \text{ mA/cm}^2$, and the self-corrosion potential reaches -1.09287 V . According to Faraday's law and obtained by Tafel extrapolation, the

corrosion rate is proportional to the corrosion current density. If the corrosion current density is lower, the corresponding corrosion rate is also lower.^{27,28} The electrochemical results showed that the corrosion resistance of HEA surfacing layers was improved after adding Ti. Ti_{0.8} exhibits the best corrosion resistance.

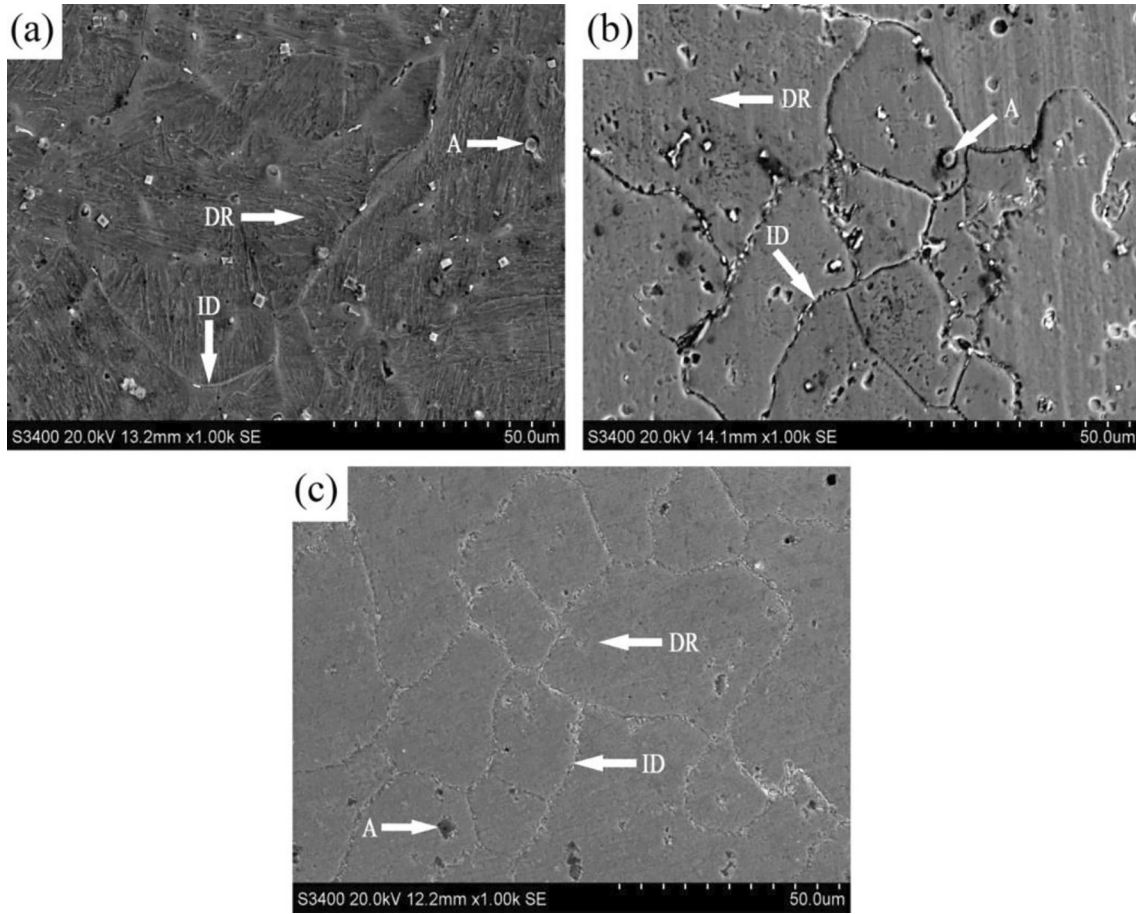


Fig. 3. Microstructure and morphology of the AlCrCuFeNiNb_{0.2}Ti_x HEAs; (a) Ti_{0.2}, (b) Ti_{0.6}, (c) Ti_{0.8}.

Table III. Element content of various regions of AlCrCuFeNiNb_{0.2}Ti_x HEA surfacing layers in Fig. 3 (at.%)

Alloys	Region	Al	Cr	Cu	Fe	Ni	Nb	Ti	C
Ti _{0.2}	Precipitates	8.46	10.21	2.88	24.64	6.54	13.37	19.56	14.34
	DR	10.75	17.99	8.95	47.04	10.74	2.36	2.17	–
	ID	10.37	10.26	22.86	28.87	7.94	6.92	12.78	–
Ti _{0.6}	Precipitates	7.29	10.12	2.36	22.07	5.66	12.54	24.69	15.27
	DR	9.60	18.34	9.41	47.08	11.07	1.67	2.73	–
	ID	9.71	9.86	23.36	24.83	8.18	6.81	17.25	–
Ti _{0.8}	Precipitates	9.98	8.79	3.51	20.01	5.62	11.16	30.67	10.26
	DR	9.34	18.64	7.86	48.56	10.58	1.85	3.17	–
	ID	10.60	9.41	26.79	17.02	8.57	7.27	20.34	–

Figure 5 shows the EIS and equivalent circuit diagram of AlCrCuFeNiNb_{0.2}Ti_x HEAs surfacing layers and 304 stainless steel in 3.5% NaCl solution. In the high-frequency region of the Nyquist plots of Fig. 5a, the impedance spectrum is a capacitance arc formed by the parallel connection of the charge transfer resistor and the capacitor. In the low-frequency region, there is no impedance caused by the diffusion process, but a semicircular inductance arc below the real axis shows that pitting corrosion occurs in the surfacing layer. In EIS, the amplitude

of the capacitance arc can reflect the corrosion resistance of materials. The larger the radius of the capacitance arc, the more corrosion resistant the materials are Ref. 29. With the continuous addition of Ti element, the corrosion rate of surfacing layers decreases gradually. Ti_{0.8} has the largest capacitance arc radius and the best corrosion resistance. In the process of corrosion, Cl⁻ in the solution induces corrosion. The passive film is constantly damaged. The impedance gradually decreases, and the capacitance arc gradually shrinks.

As shown in Fig. 5b, Bode plots show that the curve trend of AlCrCuFeNiNb_{0.2}Ti_x HEA surfacing layers are similar, which indicates that the corrosion reaction mechanism of the surfacing layers is the same. Bode plots generally focus on the impedance value in the low-frequency region. The larger the value, the better the anti-corrosion effect in the alloy.³⁰ With an increase in Ti content, the impedance value in the low-frequency region gradually increases, and the corrosion resistance effect improves. As shown in Fig. 5c, with the increase of Ti content, the phase angle in the low-frequency region gradually increases, resulting in a more dense passive film. Ti_{0.8} has the largest impedance and phase angle, and the corrosion resistance is the best.

Figure 5d shows the EIS fitting equivalent circuit diagrams of 304 stainless steel and AlCrCuFeNiNb_{0.2}Ti_x HEA surfacing layers. R_s represents the solution resistance, CPE-1 represents the electric double layer, R_{pass} represents the charge transfer resistance, Q represents the electric double layer at the interface between the passive film and the AlCrCuFeNiNb_{0.2}Ti_x HEA surfacing layer (or 304 stainless steel), R_f represents the passive film resistance, R_{sp} represents the solution resistance in the pitting area, L represents the inductance, R_{pit} represents the charge transfer resistance of the pitting region, and CPE-2 represents the capacitance of the pitting region. The fitting results are

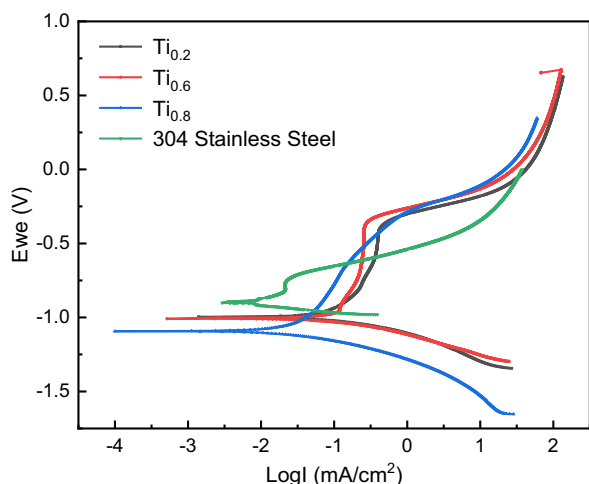


Fig. 4. Electrochemical polarization curve of the AlCrCuFeNiNb_{0.2}Ti_x HEAs.

shown in Table V, and R_{pass} is related to the stability of the passive film. The higher the R_{pass} value, the higher the corrosion resistance of the alloy.^{31,32} The higher the R_{pit} , the stronger the pitting resistance. With the continuous addition of Ti element, R_{pass} increases and the corrosion resistance of the AlCrCuFeNiNb_{0.2}Ti_x HEA surfacing layer increases.

Figure 6 shows the corrosion morphology of AlCrCuFeNiNb_{0.2}Ti_x HEA surfacing layers and 304 stainless steel. The passivation film on the upper surface of the surfacing layer is destroyed, and the corrosion occurs first in the IDs. With the increase of the content of Ti, the degree of corrosion of the surfacing layer gradually decreases. In NaCl solution, the pitting corrosion of the surfacing layer is caused by Cl⁻. After Cl⁻ is adsorbed on the surface area of the passive film, the dissolution rate of the passive film in these areas becomes very fast, the thickness of the passive film decreases, and the inductive arc in the low-frequency area of EIS shrinks with time.^{33,34} Due to the element segregation between DR and ID, the alloy grain boundary is preferentially dissolved to form intergranular corrosion. However, 304 stainless steel produced large and deep honeycombed corrosion pits with rough surfaces, forming overall corrosion. Obviously, the corrosion resistance of AlCrCuFeNiNb_{0.2}Ti_x HEAs is stronger than that of 304 stainless steel. This is because the cocktail effect and slow diffusion effect of high entropy alloy improve its corrosivity in the medium. The microstructure corrosion of AlCrCuFeNiNb_{0.2}Ti_x HEAs mostly occurs in the interdendritic region. According to the EDS composition comparison of DR and ID, the alloy segregates in the interdendritic region, which makes the poor-Cu dendrite region and the rich-Cu interdendritic region form a primary battery, leading to the preferential corrosion of the interdendritic region. On the one hand, the significant corrosion resistance is caused by the cocktail effect. The Fe-Cr solid solution phase based on the BCC structure occupies most of the volume, and the large amount of corrosion-resistant element Cr on the alloy surface can improve the stability of the passivation film in the corrosive environment, playing a good protective role in it. Because Ti is an easy passivation element, as it increases, it forms a passivation film on the surface of the alloy to prevent further corrosion. However, excessive Ti is added to the

Table IV. Corrosion parameters of the AlCrCuFeNiNb_{0.2}Ti_x HEA surfacing layers

HEAs surfacing layer	Self-corrosion potential (V)	Self-corrosion current density (mA/cm ²)
304 Stainless steel	- 0.9008	2.3549×10^{-3}
Ti _{0.2}	- 0.99957	1.3914×10^{-3}
Ti _{0.6}	- 1.00899	5.1667×10^{-4}
Ti _{0.8}	- 1.09287	9.9586×10^{-5}

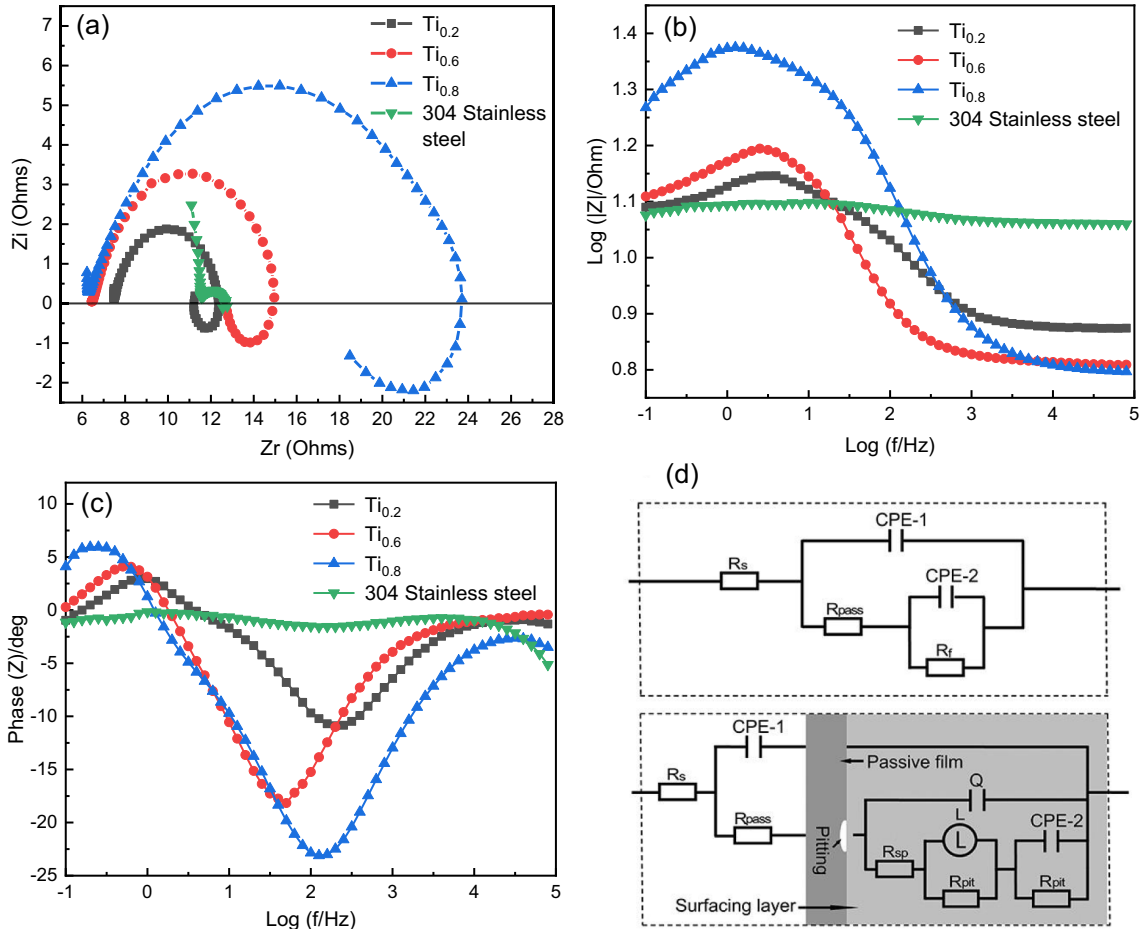


Fig. 5. EIS of the AlCrCuFeNiNb_{0.2}Ti_x HEAs; (a) Nyquist plots, (b) impedance frequency, (c) phase angle frequency, (d) equivalent current.

Table V. Equivalent circuit fitting results

Sample	R_s ($\Omega \text{ cm}^2$)	CPE-1 ($\mu\Omega^{-1} \text{ cm}^{-2} \text{ S}^{-1}$)	R_{pass} ($\Omega \text{ cm}^2$)	Q ($\mu\Omega^{-1} \text{ cm}^{-2} \text{ S}^{-1}$)	n	R_{sp} ($\Omega \text{ cm}^2$)	L (H)	R_{pit}/R_f ($\Omega \text{ cm}^2$)	CPE-2 ($\mu\Omega^{-1} \text{ cm}^{-2} \text{ S}^{-1}$)
Ti _{0.2}	0.05	$5.27e^{-9}$	0.53	$7.14e^{-4}$	0.82	3.56	0.28	1.44	$3.14e^{-4}$
Ti _{0.6}	0.01	$5.27e^{-9}$	1.63	$1.84e^{-4}$	0.78	6.04	0.60	2.76	$1.23e^{-4}$
Ti _{0.8}	0.01	$1.53e^{-8}$	6.25	$8.85e^{-4}$	0.75	9.33	2.57	5.76	$3.40e^{-2}$
304	0.39	$1.54e^{-8}$	0.16	—	—	—	—	0.98	$1.19e^{-3}$

BCC solid solution, which leads to an increase in grain size and thus improves the corrosion resistance of the alloy.^{35,36} On the other hand, significant corrosion resistance is caused by the slow diffusion effect: from the perspective of kinetics, the diffusion is slower, the corrosion rate is slower, and the corrosion resistance of the alloy is improved.^{37,38}

CONCLUSION

1. The phase structure of AlCrCuFeNiNb_{0.2}Ti_x HEA surfacing alloy is mainly Fe-Cr solid

solution with BCC structure and a tiny amount of (Nb,Ti)C with FCC structure. Its microstructure is a typical dendritic structure, and the tiny particles of composite (Nb,Ti)C are dispersed in the alloy structure. The continuous addition of Ti element is beneficial to the formation of BCC solid solution, and the BCC phase always occupies the dominant position in HEA surfacing alloy. When the Ti content is 0.8 mol, the proportion of BCC phase reaches 97.81%.

2. For the corrosion resistance of AlCrCuFeNiNb_{0.2}Ti_x HEA surfacing alloy, with the continuous addition of Ti element, the self-corrosion

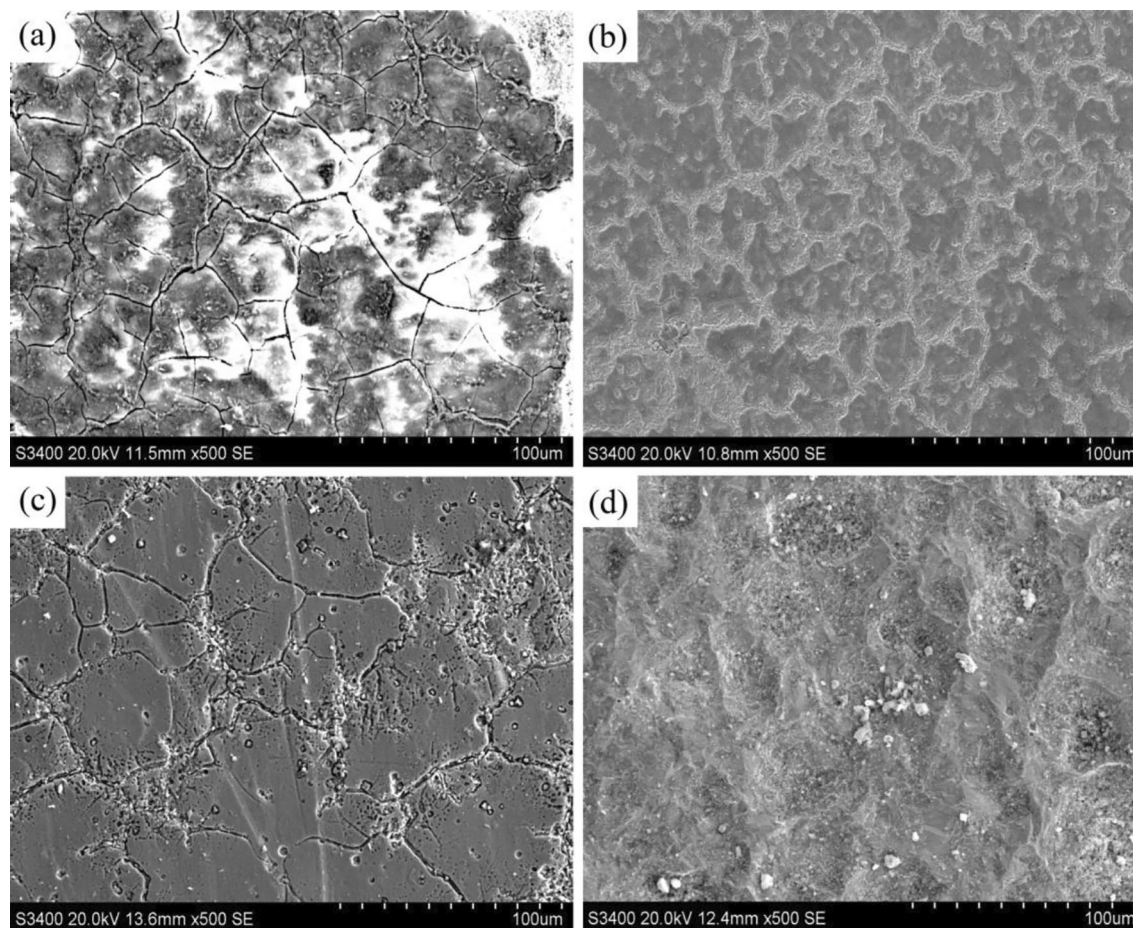


Fig. 6. Corrosion morphology of the AlCrCuFeNiNb_{0.2}Ti_x HEAs and 304 stainless steel; (a) Ti_{0.2}, (b) Ti_{0.6}, (c) Ti_{0.8}, (d) 304 stainless steel.

current density of the polarization curve decreases, the capacitance impedance radius of the impedance spectrum increases, and the corrosion resistance of the alloy increases. This leads to improved performance, better than 304 stainless steel. When the Ti content was Ti_{0.8}, the corrosion resistance of the HEA surfacing alloy was best.

- For the corrosion resistance mechanism of AlCrCuFeNiNb_{0.2}Ti_x HEA surfacing alloy, on the one hand, the addition of corrosion-resistant components Cr and Ti is conducive to the formation of a passivation film on the surface of the alloy, and the cocktail effect results in corrosion resistance of the high-entropy surfacing alloy. On the other hand, the slow kinetic diffusion effect results in corrosion resistance of the HEA surfacing alloy to be improved, the diffusion is slower, the corrosion rate is slower, and the corrosion resistance is improved.

ACKNOWLEDGEMENTS

The authors are grateful for a National Key and Program of China grant (No. 2017YFB1103603), and a Natural Science Foundation Program Key

Projects of Liaoning Province Grant (No. 20180510030).

CONFLICT OF INTEREST

On behalf of all authors, the corresponding author states that there is no conflict of interest.

REFERENCES

- J.W. Yeh, S.K. Chen, S.J. Lin, J.Y. Gan, T.S. Chin, T.T. Shun, C.H. Tsau, and S.Y. Chang, *Adv. Eng. Mater.* 6, 299 (2004).
- K.H. Huang and J.W. Yeh, A study on multicomponent alloy systems containing equal-mole elements[D]. (National Tsing Hua University, Hsinchu, 1996).
- J.W. Yeh *Ann. Chim. Sci. Mat.* 6, 633 (2006).
- Y. Zhang, T.T. Zuo, Z. Tang, M.C. Gao, K. Dahmen, P.K. Liaw, and Z.P. Lu, *Prog. Mater. Sci.* 61, 1 (2014).
- D.B. Miracle and O.N. Senkov, *Acta Mater.* 122, 448. (2017).
- S. Guo, C. Ng, J. Lu, and C.T. Liu, *J. Appl. Phys.* 109, 103505 (2011).
- Y.Y. Chen, U.T. Hong, H.C. Shih, J.W. Yeh, and T. Duval, *Corros. Sci.* 47, 2699 (2005).
- A.V. Kuznetsov, D.G. Shaysultanov, N.D. Stepanov, G.A. Salishchev, and O.N. Senkov, *Mater. Sci. Eng. A* 533, 107. (2012).
- M.H. Chuang, M.H. Tsai, W.R. Wang, and S.J. Lin, *Acta Mater.* 59, 6308 (2011).

10. N.D. Stepanov, D.G. Shaysultanov, R.S. Chernichenko, N.Y. Yurchenko, S.V. Zherebtsov, M.A. Tikhonovsky, and G.A. Salishchev, *J. Alloys Compd.* 693, 394 (2017).
11. O.N. Senkov, S.V. Senkov, D.M. Dimiduk, C. Woodward, and D.B. Miracle, *J. Mater. Sci.* 47, 6522 (2012).
12. H.P. Chou, Y.S. Chang, S.K. Chen, and J.W. Yeh, *Mater. Sci. Eng. B* 163, 184 (2009).
13. Y.J. Zhou, Y. Zhang, Y.L. Wang, and G.L. Chen, *Appl. Phys. Lett.* 90, 181904 (2007).
14. Z. Tang, L. Huang, and W. He, *Entropy* 16, 895 (2014).
15. C.M. Lin, H.L. Tsai, and H.Y. Bor, *Intermetallics* 18, 1244 (2010).
16. C.C. Juan, M.H. Tsai, C.W. Tsai, C.M. Lin, W.R. Wang, C.C. Yang, S.K. Chen, S.J. Lin, and J.W. Yeh, *Intermetallics* 62, 76 (2015).
17. Y.D. Wu, Y.H. Cai, T. Wang, J.J. Si, J. Zhu, Y.D. Wang, and X.D. Hui, *Mater. Lett.* 130, 277 (2014).
18. C.L. Wu, S. Zhang, C.H. Zhang, H. Zhang, and S.Y. Dong, *J. Alloys Compd.* 698, 761 (2017).
19. T. Fujieda, H. Shiratori, K. Kuwabara, M. Hirota, T. Kato, K. Yamanaka, Y. Koizumi, A. Chiba, and S. Watanabe, *Mater. Lett.* 189, 148 (2017).
20. H. Zhang, Y. Pan, Y.Z. He, and H.S. Jiao, *Appl. Surf. Sci.* 257, 2259 (2011).
21. Y. Zou, S. Maiti, W. Steurer, and R. Spolenak, *Acta Mater.* 65, 85 (2014).
22. Y.H. Su, X.W. Liang, Y.Q. Liu, and Z.Y. Dai, *Acta Metall. Sin. Engl. Lett.* 33, 957 (2020).
23. X.F. Li, Y.H. Feng, B. Liu, X.H. Yang, W.D. Zhang, G. Chen, Y. Liu, and P.K. Bai, *J. Alloys Compd.* 788, 454 (2019).
24. J. Liu, H. Liu, P.J. Chen, and J.B. Hao, *Surf. Coat. Technol.* 361, 63 (2019).
25. Z. Gu, S.Q. Xi, and C.F. Sun, *J. Alloys Compd.* 819, 4 (2019).
26. X.J. Shang, Q.B. Liu, and Y.X. Guo, *J. Funct. Mater.* 48, 12214 (2017).
27. C.L. Wu, S. Zhang, C.H. Zhang, H. Zhang, and S.Y. Dong, *Surf. Coat. Technol.* 315, 368 (2017).
28. Y.X. Guo, X.J. Shang, and Q.B. Liu, *Surf. Coat. Technol.* 344, 353 (2018).
29. C.N. Cao (ed.), *Introduction of Electrochemical Impedance Spectra* (Science Press, Beijing, 2002), p 70.
30. Z.H. Han, W.N. Ren, J. Yang, A.L. Tian, Y.Z. Du, G. Liu, R. Wei, G.J. Zhang, and Y.Q. Chen, *J. Alloys Compd.* 816, 152583 (2020).
31. B.S. Yilbas, I. Toor, C. Karatas, J. Malik, and I. Ovali, *Opt. Laser Eng.* 64, 17 (2015).
32. D. Szwieczek and A. Baron, *J. Mater. Process. Technol.* 164, 940 (2005).
33. Y. Li, D.Y. Lin, Y.X. Chen, and Y. Zheng, *Corros. Sci. Prot. Technol.* 28, 455 (2016).
34. Z.H. Sun, N. Zhang, J.P. Cai, M. Liu, and F. Lu, *Acta Aeron. Astronaut. Sin.* 29, 746 (2008).
35. H. Zhang, Y. Zou, Z.D. Zou, and D.T. Wu, *Opt. Laser Technol.* 65, 119 (2015).
36. J.B. Cheng, X.B. Liang, and B.S. Xu, *Surf. Coat. Technol.* 240, 184 (2014).
37. Y.F. Kao, T.D. Lee, S.K. Chen, and Y.S. Chang, *Corros. Sci.* 52, 1026 (2010).
38. G. Azimi and M. Shamanian, *J. Alloys Compd.* 505, 598 (2010).

Publisher's Note Springer Nature remains neutral with regard to jurisdictional claims in published maps and institutional affiliations.

Springer Nature or its licensor (e.g. a society or other partner) holds exclusive rights to this article under a publishing agreement with the author(s) or other rightsholder(s); author self-archiving of the accepted manuscript version of this article is solely governed by the terms of such publishing agreement and applicable law.